

Interacting bosons in generalized zigzag and railroad-trestle models

Sebastian Greschner¹ and Tapan Mishra²

¹*Department of Quantum Matter Physics, University of Geneva, 1211 Geneva, Switzerland*

²*Department of Physics, Indian Institute of Technology, Guwahati, Assam 781039, India*



(Received 19 March 2019; revised manuscript received 28 August 2019; published 2 October 2019)

We theoretically study the ground-state phase diagram of strongly interacting bosons on a generalized zigzag ladder model, the railroad-trestle (RRT) model. By means of analytical arguments in the limits of decoupled chains and the case of vanishing fillings as well as extensive DMRG calculations, we examine the rich interplay between frustration and interaction for various parameter regimes. We distinguish three different cases, the fully frustrated RRT model where the dispersion relation becomes doubly degenerate and an extensive chiral superfluid regime is found, the antisymmetric RRT with alternating π and 0 fluxes through the ladder plaquettes and the sawtooth limit, which is closely related to the latter case. We study detailed phase diagrams which include besides different single-component superfluids, the chiral superfluid phases, the two component superfluids, and different gaped phases, with dimer and a charge-density wave order.

DOI: [10.1103/PhysRevB.100.144405](https://doi.org/10.1103/PhysRevB.100.144405)

I. INTRODUCTION

Frustrated systems are one of the most interesting as well as widely explored yet still most challenging problems in the field of condensed matter physics. Frustrations in one and quasi-one-dimensional systems, such as quasi-one-dimensional magnetic materials [1–4], are of paramount importance due to the strong correlations which in interplay with the geometric frustration lead to nontrivial and intriguing physics. Theoretically in particular the J_1 - J_2 spin model, with a frustrated next-nearest neighbor tunneling amplitude J_2 , has been extensively studied during the recent decades and important milestones include the famous analytical solution for the isotropic spin-1/2 J_1 - J_2 model by Majumdar and Ghosh [5] or the Ising type phase transition between the critical Luttinger-liquid XY and the gapped dimerized (D) phase [6,7]. Detailed ground-state properties in different regimes and for various spins $S \geq 1/2$ have been discussed both numerically and analytically [8–14] in the ferromagnetic [15] as well as antiferromagnetic regime [16–18].

Recent experiments on ultracold quantum gases in optical lattices [19–22], as well as irradiated graphene [23,24] or photonic lattices [25–27], have paved the path towards the manipulation of lattice frustration to establish a situation to mimic condensed matter phenomena. The seminal experimental emulation of geometric frustration in a triangular optical lattice by Struck *et al.* [20] has attracted enormous interest to understand the physics of lattice frustration at ultralow temperature. In recent years, various interesting predictions have been made in the context of geometric frustration in low-dimensional lattices such as zigzag lattices which resembles the quantum J_1 - J_2 model under proper conditions: studies on systems of bosons in frustrated zigzag lattices have predicted the presence of chiral phases [28] whose existence have also been predicted in various bosonic ladder systems [29–34] and recently observed in cold atom experiments [35], which arise due the spontaneously breaking of the inversion symmetry of

the system. On the other hand, it has been shown that the supersolid phases can be stabilized in a system of hardcore bosons in a frustrated zigzag lattice with dipole-dipole interactions [36,37]. Recently, interesting extensions to an arbitrary rectified flux have been discussed [38].

A natural extension of the zigzag ladder is to allow for a difference in the tunneling amplitudes between upper and lower legs. One of the interesting variant of the frustrated zigzag lattice model is the sawtooth model which exhibits nontrivial physics due to the existence of a flat band. It has been shown that a solid order emerges at quarter filling in a frustrated one-dimensional sawtooth model by Huber and Altman [39] by means of an effective model valid in the flat-band regime. Interestingly, a numerical analysis of this model has shown that also a supersolid phase can be stabilized in the absence of long-range interactions [40]. The existence of this supersolid phase can be attributed to the presence of alternating flux in the consecutive plaquettes of the lattice which occurs due the lattice geometry.

In this paper, we widen the scope of study to the general railroad-trestle (RRT) model where one considers different hopping amplitudes in the legs of the ladder as shown in the Fig. 1. The RRT model and its variant the sawtooth model have been analyzed in the context of fermions [41–47], but the bosonic or spin analog of this model is still a open problem. In particular, given the interest in the sawtooth model due to unconventional transport properties and supersolidity, and a possible experimental realization of the zigzag ladder like models in the foreseeable future [38,48,49], the RRT model as asymmetric variant of the paradigmatic J_1 - J_2 model poses an interesting problem to study. In this paper, we present a detailed analysis of the ground-state properties of the bosonic RRT model in different limits to understand the effects of geometric frustration. We study three major variants of the RRT model using different analytical arguments in the limiting cases. The exact ground-state properties are studied using the density matrix renormalization group (DMRG) method [50,51].

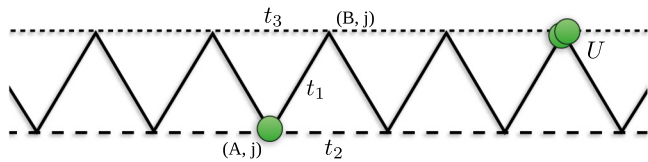


FIG. 1. Railroad-trestle (RRT) lattice which is a most general model for zigzag ladder with tunneling amplitudes t_1 , t_2 , and t_3 .

II. MODEL

The RRT model as sketched in Fig. 1 is defined by the following Hamiltonian:

$$\begin{aligned}
 H(t_1, t_2, t_3) = & -t_1 \sum_j (a_j^\dagger b_j + b_j^\dagger a_{j+1} + \text{H.c.}) \\
 & -t_2 \sum_j (a_j^\dagger a_{j+1} + \text{H.c.}) \\
 & -t_3 \sum_j (b_j^\dagger b_{j+1} + \text{H.c.}) \quad (1)
 \end{aligned}$$

Here, $a_j^{(\dagger)}$ and $b_j^{(\dagger)}$ are the bosonic annihilation (creation) operators for the upper (B) and lower (A) legs, respectively (see Fig. 1). While t_1 is the hopping amplitude between the legs, t_2 and t_3 correspond to the hoppings along the leg A and leg B, respectively. The local onsite interactions can be introduced in the model as

$$H_{\text{int}} = \frac{U}{2} \sum_{v \in \{A, B\}, j} n_j^v (n_j^v - 1), \quad (2)$$

where U is the onsite repulsion and n_j^v stands for the number operators at site j . In the following we assume the energy unit $t_1 = 1$ (unless stated otherwise) making all other physical quantities dimensionless. The primary focus of this work is to study the ground-state properties of the Model (1) in the limit of hardcore bosons ($U \rightarrow \infty$) for different values of t_2 and t_3 considering the frustrated regime, i.e., $t_2 < 0$. This assumption on the sign of t_2 introduces a π flux associated with the Peierl's phase in a plaquette. It is now useful to introduce a dimensionless parameter

$$\delta = t_3/t_2. \quad (3)$$

In the numerical treatment of the ladder, we order the lattice sites along the zigzag direction of the ladder introducing L lattice site alternating between A and B sites with bosonic operators c_l where $c_l = a_{l/2}$ if l is odd and $c_l = b_{(l-1)/2}$ for even l . With this the model (1) can be trivially rewritten

$$\begin{aligned}
 H(t_1, t_2, t_3) = & -t_1 \sum_j (c_l^\dagger c_{l+1} + \text{H.c.}) \\
 & -t_2 \sum_{l \text{ even}} (c_l^\dagger c_{l+2} + \text{H.c.}) \\
 & -t_3 \sum_{l \text{ odd}} (c_l^\dagger c_{l+2} + \text{H.c.}). \quad (4)
 \end{aligned}$$

The remaining part of the paper is organized as follows. In this section, we analyze two limiting cases of the model (1) such as the single-particle spectrum and the limit of two decoupled chains, i.e., when $|t_1| \ll |t_2|, |t_3|$. In the following

sections, we discuss three different families of parameters: Sec. III is devoted for the fully frustrated RRT(FF-RRT) model with π - π flux arrangements, i.e., $t_3 < 0$. Sec. IV constitutes the discussion on the π -0 flux case, with $t_3 > 0$. In Sec. V, we analyze the sawtooth ladder model i.e. $t_3 = 0$. In the end, we conclude in Sec. IV.

A. Single-particle spectrum

It is instructive to start the discussion of the physics of model (1) from the single-particle perspective. The kinetic part can be written in momentum space k as

$$H = - \sum_k \begin{pmatrix} a_k \\ b_k \end{pmatrix}^\dagger \begin{pmatrix} 2t_2 \cos(2k) & t_1(1 + e^{i2k}) \\ t_1(1 + e^{-i2k}) & 2t_3 \cos(2k) \end{pmatrix} \begin{pmatrix} a_k \\ b_k \end{pmatrix}. \quad (5)$$

Diagonalizing the 2×2 matrix one obtains the energy dispersion for generally two bands as

$$\begin{aligned}
 \varepsilon_{0,1}(k) = & \pm \sqrt{4t_1^2 \cos^2(k) + (t_2 - t_3)^2 \cos^2(2k)} \\
 & - (t_2 + t_3) \cos(2k) \quad (6)
 \end{aligned}$$

with the new creation and annihilation operators

$$\begin{aligned}
 \alpha_k &= \cos(\theta_k) a_k + \sin(\theta_k) b_k, \\
 \beta_k &= \sin(\theta_k) a_k - \cos(\theta_k) b_k, \quad (7)
 \end{aligned}$$

with the corresponding Bogoliubov coefficients θ_k . This expression for $\varepsilon_0(k)$ can give us insight into the physics of the system.

In general we are interested in three different cases, distinguished by the parameter $\delta = t_3/t_2$ (setting $t_2 < 0$). In Fig. 2, we show examples of the lowest band $\varepsilon_0(k)$ dispersion for three different cases of δ and for each case we consider different values of t_2 . For $\delta > 0$, the flux through every unit cell is equal to π [Fig. 2(a)]. Here the flux π corresponds to the odd number of negative tunneling amplitudes in a plaquette. Here one finds a parameter regime in which the dispersion exhibits a doubly degenerate minimum. For the case $\delta = 1$, this model corresponds to the symmetric zigzag ladder $H_S = H(t_1, t_2, t_2)$ resembling the $J_1 - J_2$ model, which has been studied extensively in the literature as discussed in the introduction. In this case, the $\varepsilon_0(k)$ possesses single and double degenerate minima as a function of t_2 and becomes quartic ($\sim (k - Q)^4$) at the so called Lifshitz-transition point, $t_2 = -1/4$.

While for small values of $-t_2 \ll 1$ the single minimum of the dispersion relation is at $k = 0$, for large values of $-t_2 \gg 1$ and $\delta \neq 1$ the dispersion relation will generally exhibit a minimum at $k = \pi/2$. We will later on associate two different single-component Luttinger-liquid phases with these two dispersion minima, the superfluid at $k = 0$ which we call the SF₀ phase, and the corresponding SF _{$\pi/2$} phase at $k = \pi/2$. The situations in which the dispersion exhibits a degenerate minimum will give rise to further interesting quantum phases discussed below in detail.

On the other hand, for $\delta < 0$, only every second plaquette exhibits a π flux while the others have zero flux. In this case, instead of a Lifshitz transition with a quartic dispersion relation, the single-particle spectrum becomes degenerate—fixing δ —only at a single point $t_2 = t_2^c$ as shown in Fig. 2(b). This

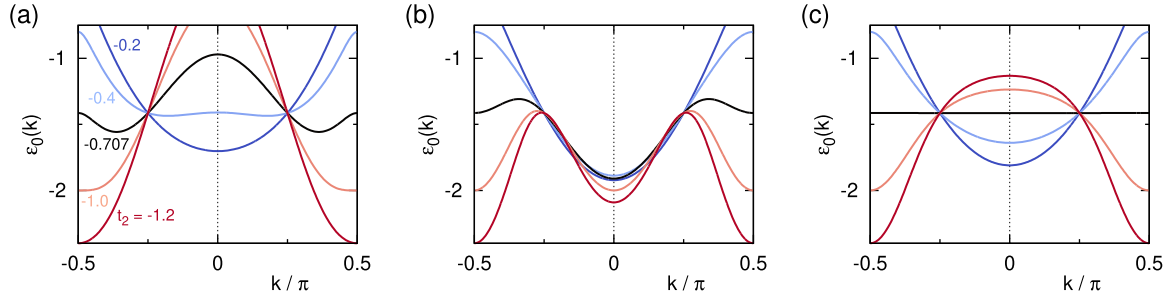


FIG. 2. Single-particle energies of the RRT model with (a) π - π -case $\delta = t_3/t_2 = 1/2$, (b) $0 - \pi$ case $\delta = -1/2$, and (c) sawtooth case $\delta = 0$. We choose $t_2 = -0.2, -0.4, -0.707, -1.0$, and -1.2 (from top to bottom at $k \rightarrow \pi/2$).

is, however, sufficient to induce a number of interesting effects in the ground-state phase diagram which we will discuss later on.

Finally, for the special case of $\delta = 0$, the system is called a sawtooth ladder. This exhibits a flat lowest band at $t_2 = -1/\sqrt{2}$ as shown in Fig. 2(c). Although apparently the sawtooth limit is the intermediate between the previous two cases, i.e., $\delta < 0$ and $\delta > 0$, this situation resembles to some extent the π -0-flux systems as one bond is absent [40]. The many-body physics which translates from this kind of band picture will be systematically discussed in the following sections.

Anticipating the results of the following discussion, in Figs. 3 and 4, we sketch the local density, current and kinetic energy configurations of the different quantum phases found in the RRT model. While fermions and bosons exhibit the same single-particle physics, the quantum phases at finite density will differ strongly. For a model of free fermions, only liquid phases corresponding to the SF_0 , the $SF_{\pi/2}$ are present. Additionally one may observe a two-component liquid phase

with four Fermi points, which will also be present in the bosonic model, the two-component superfluid phase (2SF). The inherent interaction in the hardcore boson model allows for the emergence of a chiral superfluid phase (CSF) in the regime of a degenerate dispersion minimum competing with the 2SF phase.

B. Limit of decoupled chains $|t_1| \ll |t_2|, |t_3|$

The phase diagram in the frustrated regime can be understood from the limit of two decoupled chains which is $|t_1| \ll |t_2|, |t_3|$ or in other words when $t_1 \rightarrow 0$ the two chains are independent. For an asymmetric system, i.e., if $t_2 \neq t_3$, both chains will in general be occupied by different particle densities. In the decoupling limit, we expect only one chain with the larger tunneling amplitude $t_3 > t_2$ to be occupied, if the density n is small enough. This can be seen from a mapping to free fermions, which results in two bands $-2t_2 \cos(k)$ and $-2t_3 \cos(k)$. Only the lowest band is occupied for

$$n < \arccos\left(\frac{t_2}{t_3}\right)/2\pi. \quad (8)$$

For larger fillings, the system enters a regime with two critical Luttinger liquids or two-superfluids (2SF) phase, characterized by a central charge $c = 2$ [52].

The effect of a perturbative coupling between the two chains, i.e., by adding a small zigzag hopping

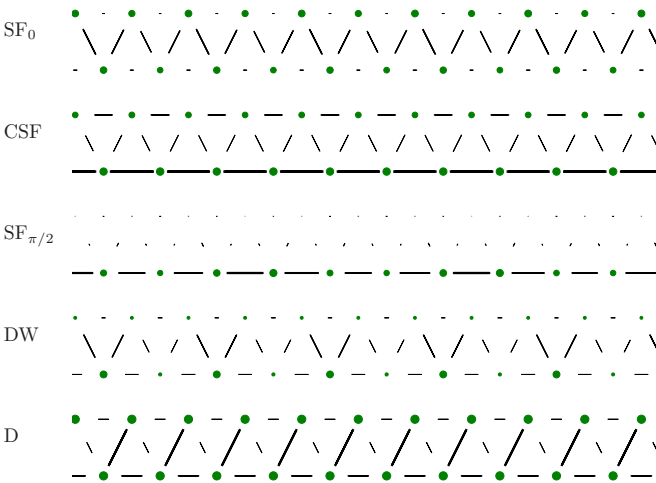


FIG. 3. Local configurations of density (size of the bullets) and bond kinetic energy (lengths and thickness of the lines) of some of the quantum phases observed on the railroad-trestle model are shown for $\delta = -1/2$. The sketches adapted from DMRG simulations are the superfluid phase at momentum $k = 0$ (SF_0), the chiral superfluid (CSF), the superfluid phase at momentum $k = \pi/2$ ($SF_{\pi/2}$), the density wave phase at quarter filling (DW) and the dimerized phase at half filling (D).

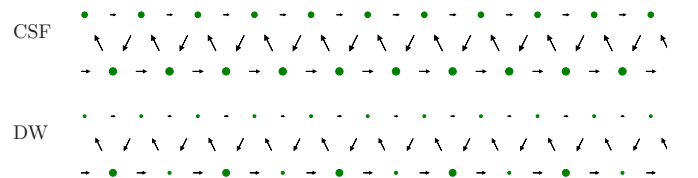


FIG. 4. Local configurations of density (size of the bullets) and local chirality or current (lengths and thickness of the arrows) of the chiral superfluid (CSF) and the density wave phase at quarter filling (DW). Sketches adapted from DMRG simulations. As discussed in the main text the nonvanishing chirality in the DW phase is probably a finite size effect. In order to visualize the chirality (in the π -flux model the local current vanishes), we manually break the symmetry by adding a small complex phase $e^{i0.01\pi}$ to next-nearest neighbor bonds—the rest of the data presented in this paper is obtained without this trick and by directly calculating the corresponding chirality correlation function.

$H_{zz} = H(t_1, 0, 0)$ is best described by a bosonization treatment of this case as presented in Ref. [9] for the symmetric case $\delta = 1$. For each subchain, we introduce two pairs of bosonic fields (θ_1, ϕ_1) and (θ_2, ϕ_2) , with $a^\dagger(b^\dagger)_j \sim \sqrt{n}e^{i\theta_{1(2)}(x)}[1 + 2\cos(2\pi nx + 2\phi_{1(2)}(x)) + \dots]$ and $x = j \cdot d$, d being the lattice spacing and the average density n . After forming symmetric and antisymmetric combinations $\theta_\pm = (\theta_1 \pm \theta_2)/\sqrt{2}$, $\phi_\pm = (\phi_1 \pm \phi_2)/\sqrt{2}$, the effective low-energy model [28] is given by

$$\mathcal{H}_S = \sum_{v=\pm} \frac{v_v}{2\pi} \left[\frac{\pi^2(\partial_x \phi_v)^2}{K_v} + K_v(\partial_x \theta_v)^2 \right] + \lambda \partial_x \theta_+ \sin \sqrt{2}\theta_- + \dots \quad (9)$$

λ , K_\pm , and v_v are phenomenological constants. The last term is relevant and introduces a gap in the anti-symmetric sector θ_- , resulting in a finite chirality $O_\chi \sim (\sin \sqrt{2}\theta_-)$ [53]. In the thermodynamic limit, it exhibits a nonvanishing local boson current or chirality $\kappa_j = \frac{i}{4}(a_j^\dagger b_j + b_j^\dagger a_{j+1} - \text{H.c.})$ in the system which is a signature of the chiral superfluid(CSF) phase. In a finite system this locally defined chirality is always zero. However, the CSF phase is clearly characterized by the long-range ordered chirality-chirality correlations defined as

$$O_\chi = \lim_{|j-j'|\rightarrow\infty} \langle \kappa_j \kappa_{j'} \rangle. \quad (10)$$

It is to be noted that the CSF phase possess a central charge $c = 1$ and the 2SF phase does not exhibit a finite chirality.

Interestingly, for the antisymmetric zigzag model $H_A = H(t_1, t_2, -t_2)$, i.e., with $\delta = -1$, we do not expect this gapping mechanism to work. This can be understood by a simple gauge transformation $a_j^{(\dagger)} \rightarrow (-1)^j a_j^{(\dagger)}$, and $b_j^{(\dagger)} \rightarrow b_j^{(\dagger)}$. With this we can map $H_A \rightarrow H_S$, but the zigzag hopping acquires an oscillating factor

$$H_{zz} \rightarrow \sum_j (-1)^j (a_j^\dagger b_j - b_j^\dagger a_{j+1} + \text{H.c.}). \quad (11)$$

Due to this strong oscillatory term, the perturbation in general becomes irrelevant and the system should stay in the 2SF phase. Only for the case of a certain commensurabilities, such as $n = 1/4$, however, the oscillation may be compensated in a bosonization description. Here, with the above nomenclature one obtains up to irrelevant terms

$$\mathcal{H}_A = \sum_{v=\pm} \frac{v_v}{2\pi} \left[\frac{\pi^2(\partial_x \phi_v)^2}{K_v} + K_v(\partial_x \theta_v)^2 \right] + \lambda' \cos \sqrt{8}\phi_+ \cos \sqrt{2}\theta_- + \dots \quad (12)$$

We may again treat the last term in a mean-field way. It is highly relevant and will open a gap as well in the symmetric sector for any finite zigzag coupling ($K_+ < 4$). Hence, we expect the emergence of a stable gapped phase which is in this case a density wave ordered phase at quarter filling for the antisymmetric model in the large $t_2 \gg t_1$ limit.

Note that the asymmetric case ($t_2 \neq t_3$) may be understood as a combination of the symmetric and antisymmetric zigzag model, i.e., $H = \frac{t_2+t_3}{2}H_S + \frac{t_2-t_3}{2}H_A + H_{zz}$. Hence, we might naively expect the physics arising as a combination of both the effects. In the following, we will examine these heuristic arguments by means of more rigorous methods.

III. THE FULLY FRUSTRATED RRT (FF-RRT) MODEL (π - π FLUX)

In this section, we begin the discussion with the case $\delta > 0$ and then we compare our results with the already known case of the symmetric zigzag chain. First we analyze the physics in the dilute limit and then we extend our calculation by increasing the density.

A. Dilute limit

The interplay between local interactions and geometric frustration which gives rise to the various quantum phases can be best understood in the limit of low fillings $n \rightarrow 0$ or the dilute limit. In the presence of two nonequivalent minima at $k = \pm Q$, the ground state of a noninteracting boson system is highly degenerate and the effect of interactions becomes crucial which selects a particular ground state. The particles at low energies mainly populate the two dispersion minima at Q and $-Q$. We can interpret them as two different bosonic flavors and map to an effective two component model with intraspecies coupling $g_{11} = g_{22}$ between bosons of the same species and interspecies coupling g_{12} between different flavors. Typically two different types of SF ground states may be stabilized: either the bosons equally occupy both minima, i.e., both flavors are present (the 2SF phase), or one of them is spontaneously selected and a one component SF phase with a spontaneously broken symmetry is realized.

If the intraspecies coupling $g_{11} > g_{12}$, a two component Luttinger-liquid phase (2SF) may be realized. In this case both the dispersion minima are equally populated. On the other hand a dominant interspecies coupling $g_{11} < g_{12}$ results a spontaneously broken state with a dominant occupation of the dispersion minimum at $k = Q$ or $k = -Q$.

While in general it is a useful observation [14] that both coupling coefficients, g_{11} and g_{12} , may be extracted from the two particle scattering problem on the lattice, here we will follow a slightly different approach. As shown in Ref. [14] in the dilute limit it is possible to obtain the renormalized intra- and intercomponent interactions analytically as an exact solution of the corresponding Bethe-Salpeter equation. A detailed analytical treatment can be found in Ref. [14].

For simplicity, we will project the interaction to the lowest band. In momentum space, the Hamiltonian becomes

$$H = \sum_k \epsilon(k) \beta_k^\alpha (\beta_k^\alpha)^\dagger + \frac{1}{2L} \sum_{k,k',q} V_q(k, k') \beta_{k+q}^\dagger \beta_{k'-q}^\dagger \beta_k \beta_{k'}, \quad (13)$$

where $V_q(k, k')$ is the interaction in the lowest band in the momentum representation and the operator β has been introduced in Eq. (7). For a local Bose-Hubbard model like interaction Eq. (2), this is given by

$$V_q(k, k') = \frac{U}{2} (\cos(\theta_k) \cos(\theta_{k'}) \cos(\theta_{k'-q}) \cos(\theta_{k+q}) + \sin(\theta_k) \sin(\theta_{k'}) \sin(\theta_{k'-q}) \sin(\theta_{k+q})). \quad (14)$$

While for the rest of the paper we discuss properties of $U \rightarrow \infty$, here we use finite interactions and extrapolate afterwards to the hardcore limit.

We obtain the renormalized two-body interactions Γ_{11} and Γ_{12} in the dilute limit by the following form of the Bethe-Salpeter equations

$$\Gamma_q^{11}(E) = V^{11}(Q, 0) - \frac{1}{L} \sum_p \frac{V^{11}(q, p) \Gamma_p^{11}(E)}{\epsilon_{Q+p} + \epsilon_{Q-p} - E} \quad (15)$$

and

$$\Gamma_q^{12}(E) = 2V^{12}(q, Q) - \frac{1}{L} \sum_p \frac{V^{12}(q, p) \Gamma_p^{12}(E)}{2\epsilon_p + E}, \quad (16)$$

where E is the total energy of the incoming particles with momentum k and k' . Here we have introduced the symmetrized interactions

$$\begin{aligned} V^{11}(q, p) &= \frac{1}{2}(V_{q-p}(Q+p, Q-p) + V_{q+p}(Q-p, Q+p)), \\ V^{12}(q, p) &= \frac{1}{2}(V_{q-p}(-p, p) + V_{q+p}(p, -p)). \end{aligned} \quad (17)$$

Γ_{11} and Γ_{12} may be related to the bare coupling strengths g_{11} and g_{12} as

$$\frac{1}{\Gamma_{\alpha\beta}(-E_*)} = \left(\frac{m}{4E_*}\right)^{1/2} + \frac{1}{g_{\alpha\beta}} + \mathcal{O}(E_*^{1/2}), \quad (18)$$

which corresponds to an off-shell regularization introducing a negative energy E_* . For $E_* \rightarrow 0$, corresponding to the dilute limit this procedure has been shown to be well defined. In the following we directly solve Eqs. (15) and (16) numerically by introducing a Fourier representation of $\Gamma_q^{\alpha\beta}(-E_*)$ using a discretization of the equation and subsequent fast Fourier transform algorithm. The resulting linear set of equation can be solved using standard methods for finite values $E_* > 0$ and subsequent extrapolation to $E_* \rightarrow 0$. This procedure becomes eventually unstable due to the presence of divergences in $\Gamma_q^{\alpha\beta}(E_*)$.

In Fig. 5, we show the coupling constants as function of U for the case $t_2/t_1 = 0.6$ and $\delta = 0.5$. We extrapolate $g_{\alpha\beta}$ with a third order polynomial to the limit $E_* \rightarrow 0$. For weak interactions the interspecies couplings dominate. At a finite $U > U_c$, we observe a crossing between g_{11} and g_{12} curves and hence, a transition to the intraspecies coupling dominated 2SF phase. In the inset of Fig. 5, we show the extracted transition points $U = U_c$ as a function of δ for the case $t_2 = -0.6$. It can be seen that as the value of δ increases the CSF phase becomes more robust and survives even in the large U limit.

Now we perform numerical DMRG simulations to compare the results with the above findings for the example $t_2 = -0.6$, also shown in Fig. 5. By considering a system of hardcore bosons with a finite but small filling $n = 0.1$, we compute different order parameters such as the chirality order parameter O_χ as defined from the large distance properties of the chirality-chirality correlations of Eq. (10) and the momentum distribution function $n(k)$. The momentum distribution function is defined along the zigzag direction of the lattice as

$$n(k) = \frac{1}{L^2} \sum_{l,l'} e^{ik(l-l')} G_{ll'} \quad (19)$$

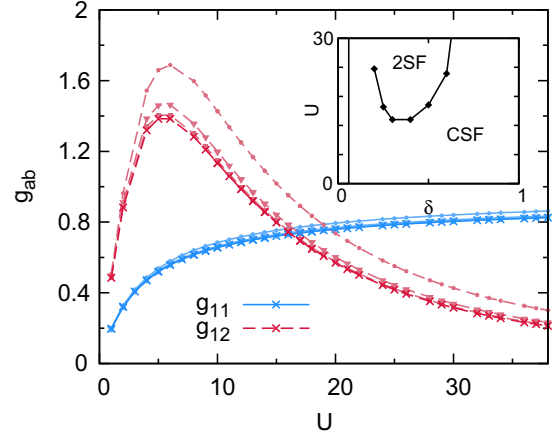


FIG. 5. Dilute limit intra-(inter)particle coupling constants $g_{11}(g_{12})$ are plotted with respect to U for $t_2 = -0.6$ and $\delta = 0.5$. Different curves correspond to (top to bottom) different values of $E_* = 10^{-2}, 10^{-3},$ and 10^{-4} and the cross-symbol denotes the extrapolation to $E_* \rightarrow 0$. It can be seen that the value of g_{11} dominates over g_{12} after a critical value of U indicating the 2SF phase. The inset shows the phase transition points between the dominant g_{11} and g_{12} corresponding to the 2SF and the CSF phases respectively as function of U and δ for $t_2 = -0.6$. The solid vertical line denotes the Lifshitz transition between SF_0 and frustrated phases. Close to this region our numerical scheme becomes unstable.

with the single-particle Green's functions $G_{ll'} = \langle c_l^\dagger c_{l'} \rangle$ along the zigzag direction of the chain. In Fig. 6, we plot both O_χ and the peak position of $n(k)$ as a function of δ . One may clearly distinguish three regimes. For small values of δ , there exists one peak in the momentum distribution indicating an SF phase. At some $\delta > \delta_{c1}$, the momentum distribution acquires a double peak structure with $k \neq 0$ which is a signature of the 2SF phase. For $\delta > \delta_{c2}$, the chirality becomes finite and the system enters into the CSF phase.

Moreover, entanglement properties have been shown to provide useful general measure for the detection of quantum phase transitions [54,55]. In this regard, we calculate the

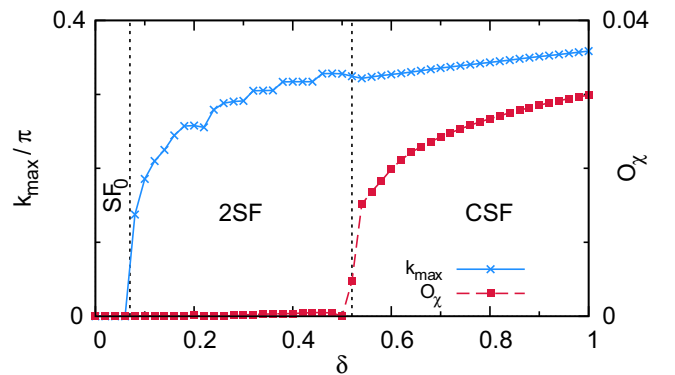


FIG. 6. Chirality O_χ and peak position k_{\max} of the momentum distribution $n(k)$ for the fully frustrated RRT model as function of $\delta > 0$ for small fillings ($n = 0.1, t_2 = -0.6$, DMRG data, $L = 80$). As $k_{\max} \neq 0$, two equivalent maxima at $\pm k_{\max}$ are found.

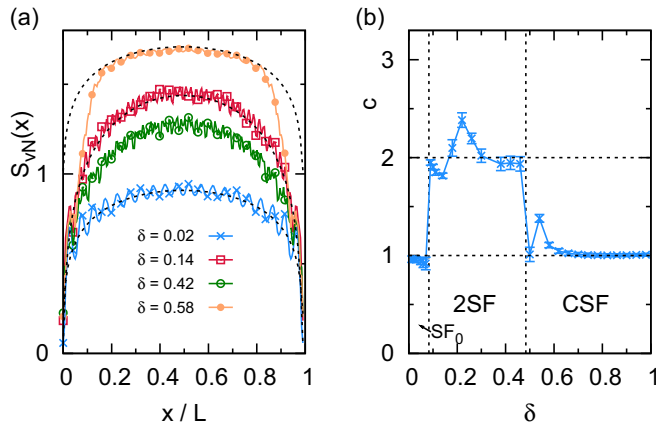


FIG. 7. Entanglement scaling for the RRT model using the same parameters as in Fig. 6 (DMRG data, $t_2 = -0.6$, $L = 201$ sites, filling $n = 0.1$). (a) Entanglement entropy $S_{vN}(x)$ for different bipartitions of the system x for various values of δ . The black dashed lines depict a fit to Eq. (20). (b) The extracted central charge c from the fitting procedure.

von-Neumann entropy which is defined as

$$S_{vN,L}(x) = -\text{tr}(\rho_x \ln \rho_x) = \frac{c}{6} \ln \left[\frac{L}{\pi} \sin \left(\frac{\pi}{L} x \right) \right] + g, \quad (20)$$

where ρ_x is the reduced density matrix for a subsystem of length x which is plotted as function of x/L in Fig. 7(a). The right part of Eq. (20) is valid for conformally invariant gapless states [52,55]. We fit the expression in the right-hand side of Eq. (20) to the entanglement entropy curves obtained using the DMRG method as shown in Fig. 7(a). From this we extract the central charge c of the underlying field theory which is shown in Fig. 7(b). Note that for the RRT model, we perform simulations of system sizes with odd number of sites in order to restore proper inversion symmetry at a central bond. Consistent with our proceeding discussion in Fig. 6, we find that the intermediate nonchiral region exhibits a central charge $c = 2$ and hence, can be called a 2SF phase.

For the special case of a symmetric zigzag model $\delta = 1$, we repeat this analysis in the dilute limit and using the DMRG method and obtain the phase diagram in the U - t_2 plane which is shown in Fig. 8. Close to the Lifshitz transition the 2SF phase is realized. For large frustrations $|t_2| > 1/\sqrt{8}$, no 2SF phase is found and the system is in a CSF phase, which remains true for the hardcore bosons case. We compare our findings to DMRG results for various fillings and interaction strengths and, as shown in the figure, find a good qualitative agreement between the two results. The symbols in Fig. 8 shows the 2SF-CSF phase boundaries for different densities such as $n = 0.05$ (cross), 0.1 (squares), and 0.2 (triangles). Note that a direct comparison between the two methods may become difficult as for finite dilute systems the order parameter, i.e., the chirality vanishes.

B. Finite densities

In this section, we will analyze the complete ground-state phase diagram of the asymmetric FF-RRT model for a fixed $\delta = 1/2$ as function of the chemical potential μ to understand

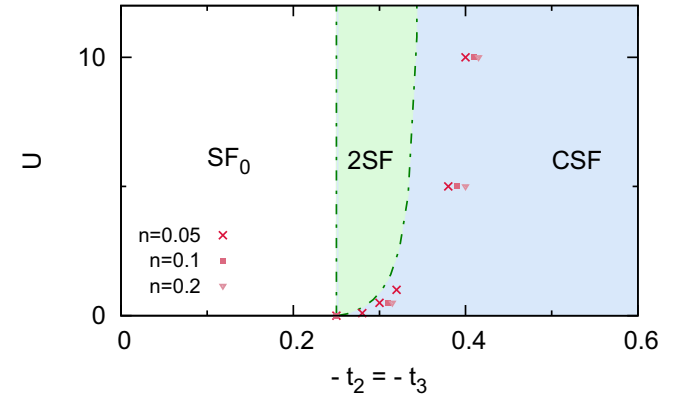


FIG. 8. Dilute limit phase diagram of interacting bosons in the symmetric zigzag model ($\delta = 1$). The dash-dotted lines stem from the dilute-limit analysis presented above. The data points show results for the 2SF to CSF transition from DMRG simulations at finite density $n > 0$.

the physics at finite densities. From the previous section, we find that if $\delta = 1/2$ for $\sqrt{\frac{3\sqrt{33}}{2} - \frac{17}{2}} < -t_2 < 1$, the lowest band in Eq. (6) has a twofold degenerate minimum at $Q = \pm \frac{t_1(3\sqrt{2t_1^2 - t_2^2} - 4t_1)}{t_2^2}$. We explore the physics of this system for different values of t_2 by varying the chemical potential μ . In Fig. 9, we show the phase diagram in the μ - t_2 plane. Consistent with the proceeding section we do not find the emergence of a CSF phase at small values of δ in the dilute limit. However, at larger fillings, the system enters an extensive CSF region. Apart from this, other interesting features appear in the phase diagram which we discuss below.

The phase transition points can be best read from the μ - n diagrams of finite systems which is shown in Fig. 10 for different values of t_2 . At the transition points between the single-component superfluid phases such as the SF and the $SF_{\pi/2}$ phases and the CSF or 2SF phases, the μ - n curve exhibits a sharp kink. In order to distinguish the 2SF and CSF phases, we use the chirality order parameter and the

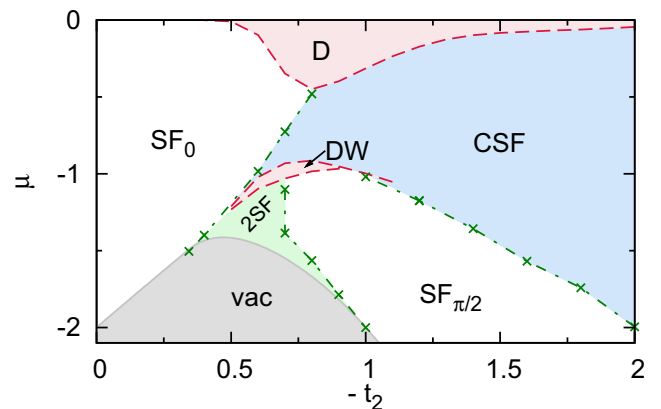


FIG. 9. Phase diagram of the FF RRT model for $\delta = 1/2$ as a function of $t_2 = 2t_3$ and the chemical potential μ . The dot-dashed lines correspond to the commensurate-incommensurate transitions. At fixed densities the transitions to the gapped phases is of Berezinsky-Kosterlitz-Thouless (BKT)-type.

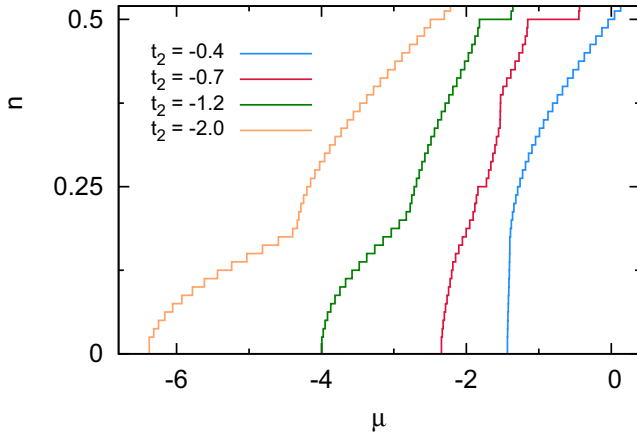


FIG. 10. μ - n curve for cuts through phase diagram Fig. 9 for $\delta = 1/2$ and (from left to right) $t_2 = -2.0, -1.2, -1.0,$ and -0.7 . The curves have been shifted by 0.8 against each other along the x axis for clarity.

central charge as discussed before. We observe the $SF_{\pi/2}$ -CSF transition for a critical density $n_c \approx 0.18$ (for $t_2 = -2$) which is consistent with $n_c = 1/6$ that is already obtained in the decoupled chain limit using Eq. (8).

The μ - n curves of Fig. 10 show a series of plateaus at certain commensurate fillings, $n = 1/4$ and $1/2$. These correspond to the gaped insulating phases, a density wave (DW) phase (at $n = 1/4$) and a dimerized (D) phase ($n = 1/2$), which are stabilized due to frustration and asymmetry of the model. As discussed in Ref. [28], at the Lifshitz transition, the band curvature vanishes locally as the minimum becomes quartic. Hence, as the effective mass diverges we may expect the pinning of particles at weak interaction strengths resulting into the emergence of gaped phases. In Fig. 9, we show the approximate extent of the plateau regions bounded by the dashed curves which are calculated for several finite system sizes and then extrapolated to the thermodynamic limit by means of a higher order polynomial. For the case of hardcore bosons, the presence of a D phase at half filling $n = 1/2$ (for zero magnetic field in the case of the corresponding spin-1/2 model) has been discussed extensively [7,12]. Following Okamoto and Nomura [7] we may extract the phase transition points between the SF_0 and the D phase by means of a level crossing analysis. To further characterize the D phase we compute the dimer-dimer order parameter as

$$O_D = \frac{1}{L} \sum_j (-1)^j B_j, \quad (21)$$

where $B_j = \langle b_j(b_{j+1}^\dagger + b_{j-1}^\dagger) \rangle$ is the bond energy. In Fig. 11(a), we show the behavior of O_D at half filling as a function of t_2 for different system sizes $L = 20, 40, 80,$ and 160 along with the extrapolated curve in the thermodynamic limit.

Interestingly, for the RRT model we also find an emerging density wave (DW) phase at quarter filling $n = 1/4$ close to the Lifshitz line. The emerging DW order can be seen as a peak in the density structure factor

$$S(k) = \frac{1}{L^2} \sum_{i,j} e^{ik(i-j)} \langle n_i n_j \rangle, \quad (22)$$

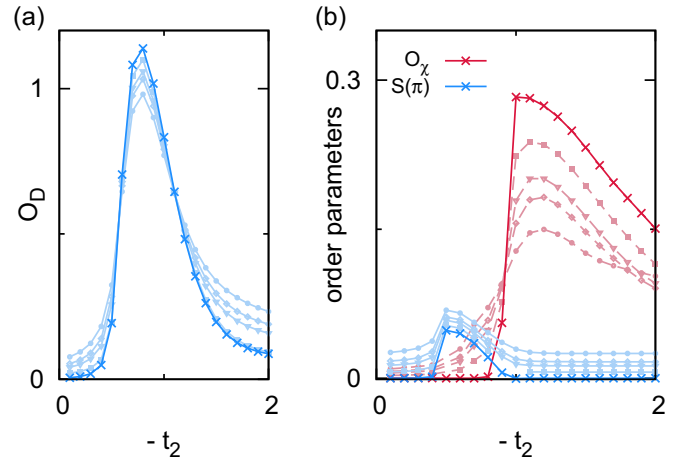


FIG. 11. Order parameters for different cuts through the phase diagram for (a) $n = 1/2$ and (b) $1/4$. The curves in lighter shadings show the finite-size results for $L = 20$ (circle), 40 (diamond), 80 (triangle), and 160 (box) sites—cross-symbols depict the extrapolation to the thermodynamic limit using a higher-order polynomial.

where $\langle n_i n_j \rangle$ is the density-density correlation between sites i and j . In Fig. 11(b), we plot the values of $S(k = \pi)$ (blue symbols) and the chirality O_χ (red symbols) as a function of t_2/t_1 for different lengths and also in the thermodynamic limit at $n = 1/4$. This clearly shows the presence of the DW phase for some intermediate range of t_2 and the system possesses finite chirality for larger values of t_2 where a CSF phase is found. Note that the chirality becomes finite abruptly with the vanishing of the DW-order parameter as we enter the CSF phase.

The phase transitions between SF_0 , $SF_{\pi/2}$ and the 2SF or CSF phases are of commensurate-incommensurate type, indicated by a kink in the n - μ curve of Fig. 10. These transitions are denoted by dash-dotted lines in Fig. 9. At fixed densities the transitions to the gaped D or DW phases are of Berezinsky-Kosterlitz-Thouless (BKT)-type transitions.

C. Symmetric zigzag model

Contrary to the previously discussed case, for the symmetric zigzag model ($\delta = 1$), the dispersion relation is doubly degenerate for every $-t_2 > 1/4$. For completeness, we depict the corresponding phase diagram in Fig. 12. Here, we find an extended CSF phase for any filling as $-t_2$ is large enough. For small densities, close to the Lifshitz transition the interesting interplay between the 2SF and CSF phases is observed. The transition point from the low-density description is consistent with the numerical simulations. Due to the symmetry of the model the DW phase at quarter filling is absent. However, there exists a D phase at $n = 1/2$ as a result of frustration.

IV. THE π -0 CASE

Let us now turn to the anti-symmetric case when $\delta < 0$, i.e., a model with a π flux through every second plaquette. Here we analyze this model along the line discussed above and obtain the complete phase diagram as shown in Fig. 13 for $\delta = -0.5$. The phase diagram is obtained by analyzing the

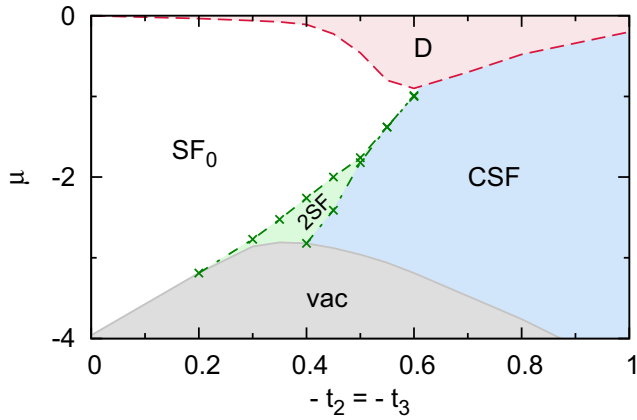


FIG. 12. Phase diagram for hardcore bosons in a symmetric frustrated zigzag ladder ($\delta = 1$) in the $t_2 = t_3$ and μ plane.

plateaus in the μ - n plot (Fig. 14) and the order parameters as done in the previous case. Figure 14 shows the emergence of plateaus only at $n = 1/4$ which corresponds the DW phase. This DW phase is denoted by the region bounded by the dashed curve in Fig. 13. Interestingly a gapped phase at half filling is absent in this case. The extent of the DW phase is drastically enhanced compared to the case of a π - π flux. In particular, for large values of $-t_2$, we still observe a finite gap after extrapolation of our numerical data to the thermodynamic limit. The grey region bounded by the continuous line is the empty state.

As discussed in Sec. II, there should not exist a CSF phase in this scenario for weakly coupled chains, which we find to remain valid also for a finite interleg hopping. We confirm this using our DMRG calculation and indeed, we see a broad region of the 2SF phase around the gapped DW phase marked by the dashed-cross boundary. The transition to the 2SF phase is characterized by a series of kinks in the μ - n curve (see Fig. 13).

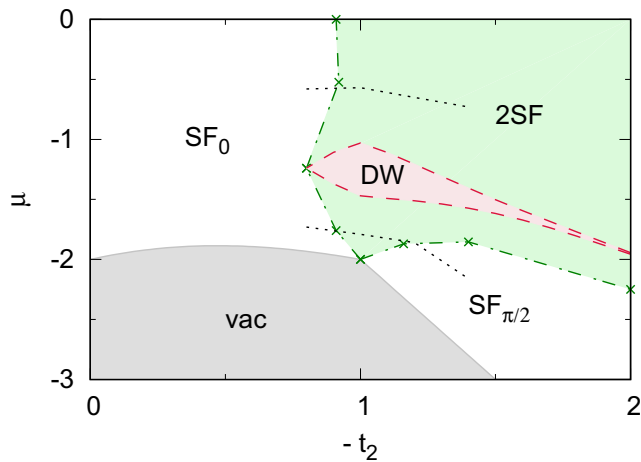


FIG. 13. Phase diagram of the π -0 RRT model with $\delta = -1/2$. The dot-dashed lines correspond to commensurate-incommensurate transitions. At fixed density the transition to the gapped phase is of BKT-type. The dotted lines correspond to $n = 1/8$ and $3/8$.

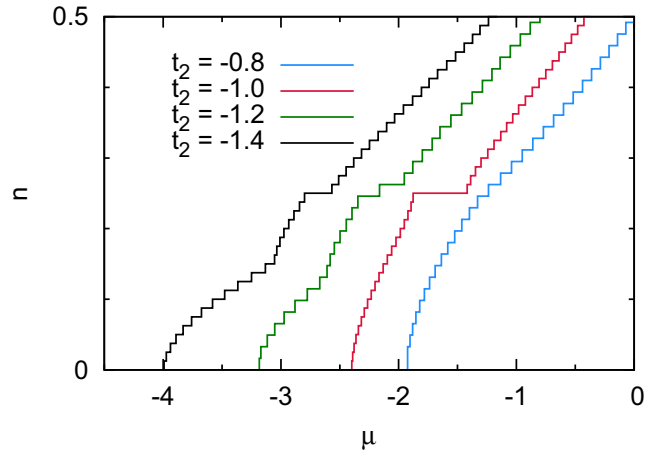


FIG. 14. μ - n curve for cuts through phase diagram of Fig. 13 for $\delta = -1/2$ and $t_2 = -1.4, -1.2, -1.0$, and -0.8 (from left to right). The curves have been shifted by 0.4 against each other along the x axis for clarity.

The SF_0 and $SF_{\pi/2}$ phases are best understood by looking at the momentum distribution function $n(k)$ as plotted in Fig. 15. We plot $n(k)$ for two cuts through the phase diagram of Fig. 13 along the x axis which correspond to two different fillings $n = 1/8$ and $3/8$ in Figs. 15(a) and 15(b), respectively. For the cut along $n = 1/8$, the momentum distribution exhibits one peak at k_0 , then three peaks and in the end two peaks at $k = \pm\pi/2$ as a function of t_2 . While the $SF_{\pi/2}$ phase is characterized by peaks at $k = \pm\pi/2$, which are equivalent, in the 2SF phase region we find multipeak structure with peaks at $k = 0$ and $\pm\pi/2$. This means the system goes from the SF to the 2SF phase and then to the $SF_{\pi/2}$ phase. In the case of $n = 3/8$, there is a single transition from the SF to the 2SF phase as can be seen from Fig. 15(b). The phase transitions between these superfluid phases are marked by the vertical dashed lines in Fig. 15. We also compute the central charge c following the analysis done in the previous section and show that the numerical estimation of the central charge is consistent with $c = 1$ in the SF_0 and $SF_{\pi/2}$ phases where as $c = 2$ in the 2SF regions (see Fig. 16).

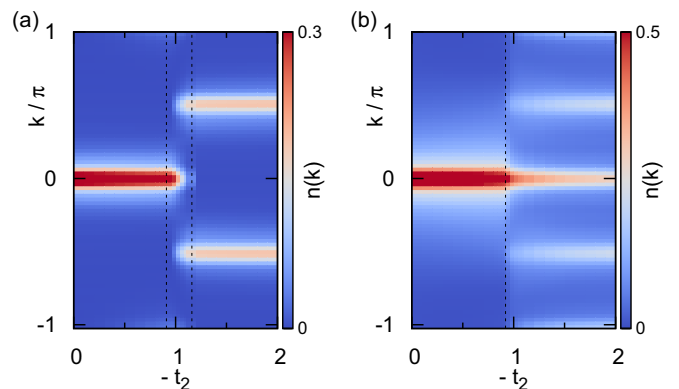


FIG. 15. Momentum distributions for filling $n = 1/8$ and $3/8$ which corresponds to two cuts indicated by dotted lines in the phase diagram of Fig. 13.

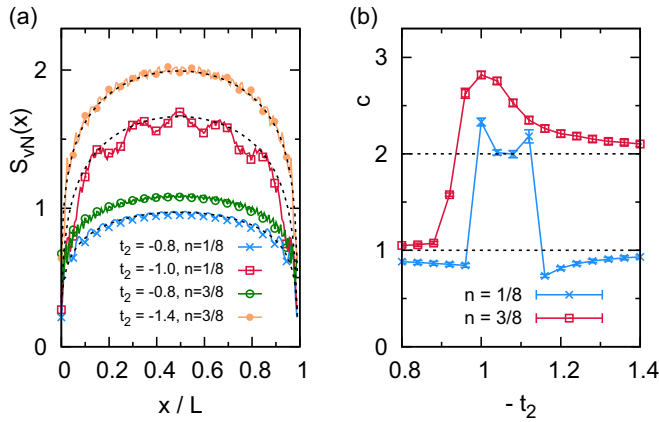


FIG. 16. Entanglement scaling for the $\delta < 0$ RRT model using the same parameters as in Fig. 6 (DMRG data, $L = 201$ sites, filling $n = 0.1$). (a) Entanglement entropy $S_{vN}(x)$ for different bipartitions of the system x for various values of δ . The black dashed lines depict a fit to Eq. (20). (b) The extracted central charge c from the fitting procedure.

V. THE SAWTOOTH CHAIN

In the end, we analyze the very special case of the RRT model which is known as the sawtooth chain. As stated in the introduction, for the sawtooth case ($\delta = 0$) the lowest band becomes exactly flat at the special value of $t_2 = -1/\sqrt{2}$ [see Fig. 2(c)]. Here we analyze the sawtooth model for the hardcore bosons case and obtain the interesting ground-state phase diagram which is shown in Fig. 17. Examples of the equation of state from which the main results can be deduced are shown in Fig. 18.

The presence of the flat band leads, as for the Lifshitz transitions, to an enhancement of correlations. As a result we find an extensive D and DW phase around $t_2 = -1/\sqrt{2}$ which are bounded by the dashed curves in Fig. 17 at $n = 1/2$ and $1/4$, respectively. The presence of the flat-band also leads to macroscopically large jumps in density in the μ - n curve for fillings below $n = 1/4$. The transition between the SF and $SF_{\pi/2}$ phase is apparently direct, possibly of first order. For

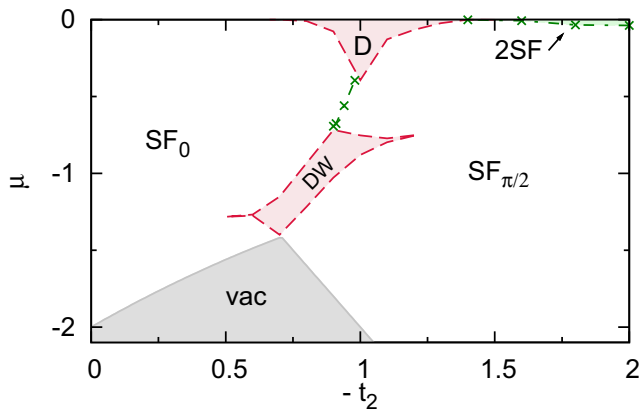


FIG. 17. The phase diagram for the sawtooth ladder model for hardcore bosons. Our simulation data suggests a direct first-order transition between the SF_0 and $SF_{\pi/2}$ phases for $1/4 < n < 1/2$.

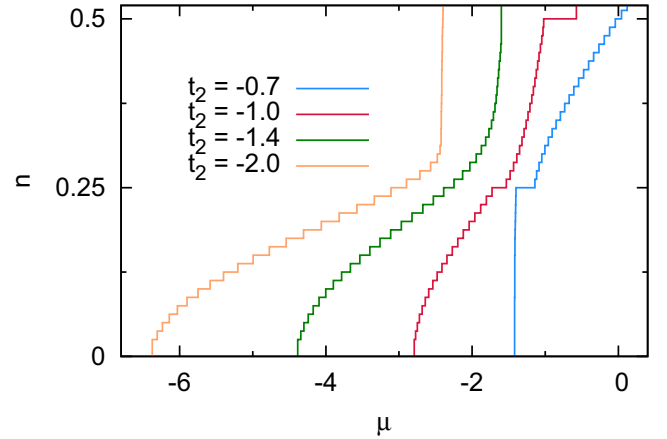


FIG. 18. μ - n curve for $t_2 = -0.7, -1.0, -1.4$, and -2.0 (right to left) for the sawtooth model. The curves have been shifted by 0.8 against each other along the x axis for clarity.

the hardcore case, we do not observe an emerging supersolid phase like the soft-core case discussed in Ref. [40], however, we find a 2SF phase for large fillings and $-t_2 \gtrsim 1.4$. As seen in Fig. 18, it is characterized by a sharp increase in the density which indicates a very large but finite compressibility.

VI. SUMMARY

In summary, in this paper, we have studied the ground-state physics of a very generic zigzag ladder model, with asymmetric hopping strengths on the two legs. The interplay between this asymmetry and the interactions of the bosonic particles gives rise to various phenomena and quantum phases including the 2SF and the CSF phases and different single-component SF phases. At certain commensurate fillings density wave and dimerized phases can be observed. While for the symmetric case chiral phases dominate the grand canonical phase diagram, the asymmetry tends to stabilize the 2SF phases.

In state of the art ultra-cold atom experiments the RRT models should in a natural way emerge from the attempts to study the symmetric zigzag ladder models. For example one may realize a zigzag model by means of superlattice techniques on triangular lattices in combination with lattice shaking [20,28]. A slight misalignment of superlattice and the triangular lattice might typically lead to the tunneling asymmetry described here. Also one might adapt synthetic dimension approaches as recently proposed in Ref. [38], where the requirement of a state-dependent lattice also may be naturally exploited to generalize to RRT-type models.

ACKNOWLEDGMENTS

We would like to thank Luis Santos and Temo Vekua for important discussions. S.G. acknowledges support of the German Research Foundation DFG (Project No. SA 1031/10-1) and of the Swiss National Science Foundation under Division II. T.M. acknowledges hospitality of the Institute for Theoretical Physics, Leibniz University

Hannover, where part of this work has been carried out and also DST-SERB for the early career grant through Project No.

ECR/2017/001069. Simulations were carried out on the cluster system at the Leibniz University of Hannover, Germany.

-
- [1] M. Hase, H. Kuroe, K. Ozawa, O. Suzuki, H. Kitazawa, G. Kido, and T. Sekine, *Phys. Rev. B* **70**, 104426 (2004).
- [2] T. Masuda, A. Zheludev, B. Roessli, A. Bush, M. Markina, and A. Vasiliev, *Phys. Rev. B* **72**, 014405 (2005).
- [3] S.-L. Drechsler, O. Volkova, A. N. Vasiliev, N. Tristan, J. Richter, M. Schmitt, H. Rosner, J. Málek, R. Klingeler, A. A. Zvyagin, and B. Buchner, *Phys. Rev. Lett.* **98**, 077202 (2007).
- [4] A. Vasiliev, O. Volkova, E. Zvereva, and M. Markina, *npj Quantum Mater.* **3**, 18 (2018).
- [5] C. K. Majumdar and D. K. Ghosh, *J. Math. Phys.* **10**, 1388 (1969).
- [6] F. D. M. Haldane, *Phys. Rev. B* **25**, 4925 (1982).
- [7] K. Okamoto and K. Nomura, *Phys. Lett. A* **169**, 433 (1992).
- [8] A. K. Kolezhuk, *Phys. Rev. B* **62**, R6057 (2000).
- [9] P. Lecheminant, T. Jolicoeur, and P. Azaria, *Phys. Rev. B* **63**, 174426 (2001).
- [10] T. Vekua, G. I. Japaridze, and H.-J. Mikeska, *Phys. Rev. B* **67**, 064419 (2003).
- [11] T. Hikihara, M. Kaburagi, H. Kawamura, and T. Tonegawa, *J. Phys. Soc. Jpn.* **69**, 259 (2000).
- [12] T. Hikihara, M. Kaburagi, and H. Kawamura, *Phys. Rev. B* **63**, 174430 (2001).
- [13] T. Hikihara, *J. Phys. Soc. Jpn.* **71**, 319 (2002).
- [14] A. K. Kolezhuk, F. Heidrich-Meisner, S. Greschner, and T. Vekua, *Phys. Rev. B* **85**, 064420 (2012).
- [15] T. Hikihara, L. Kecke, T. Momoi, and A. Furusaki, *Phys. Rev. B* **78**, 144404 (2008).
- [16] T. Hikihara and A. Furusaki, *Phys. Rev. B* **69**, 064427 (2004).
- [17] S. Furukawa, M. Sato, and S. Onoda, *Phys. Rev. Lett.* **105**, 257205 (2010).
- [18] M. Azimi, L. Chotorlishvili, S. K. Mishra, S. Greschner, T. Vekua, and J. Berakdar, *Phys. Rev. B* **89**, 024424 (2014).
- [19] M. Aidelsburger, M. Atala, S. Nascimbène, S. Trotzky, Y.-A. Chen, and I. Bloch, *Phys. Rev. Lett.* **107**, 255301 (2011).
- [20] J. Struck, C. Ölschläger, M. Weinberg, P. Hauke, J. Simonet, A. Eckardt, M. Lewenstein, K. Sengstock, and P. Windpassinger, *Phys. Rev. Lett.* **108**, 225304 (2012).
- [21] H. Miyake, G. A. Siviloglou, C. J. Kennedy, W. C. Burton, and W. Ketterle, *Phys. Rev. Lett.* **111**, 185302 (2013).
- [22] M. Aidelsburger, M. Atala, M. Lohse, J. T. Barreiro, B. Paredes, and I. Bloch, *Phys. Rev. Lett.* **111**, 185301 (2013).
- [23] T. Oka and H. Aoki, *Phys. Rev. B* **79**, 081406(R) (2009).
- [24] Y. Wang, H. Steinberg, P. Jarillo-Herrero, and N. Gedik, *Science* **342**, 453 (2013).
- [25] M. Hafezi, E. A. Demler, M. D. Lukin, and J. M. Taylor, *Nat. Phys.* **7**, 907 (2011).
- [26] M. C. Rechtsman, J. M. Zeuner, Y. Plotnik, Y. Lumer, D. Podolsky, F. Dreisow, S. Nolte, M. Segev, and A. Szameit, *Nature* **496**, 196 (2013).
- [27] S. Mittal, S. Ganeshan, J. Fan, A. Vaezi, and M. Hafezi, *Nat. Photon.* **10**, 180 (2016).
- [28] S. Greschner, L. Santos, and T. Vekua, *Phys. Rev. A* **87**, 033609 (2013).
- [29] A. Dhar, M. Maji, T. Mishra, R. V. Pai, S. Mukerjee, and A. Paramekanti, *Phys. Rev. A* **85**, 041602(R) (2012).
- [30] A. Dhar, T. Mishra, M. Maji, R. V. Pai, S. Mukerjee, and A. Paramekanti, *Phys. Rev. B* **87**, 174501 (2013).
- [31] A. Tokuno and A. Georges, *New J. Phys.* **16**, 073005 (2014).
- [32] D. Hügel and B. Paredes, *Phys. Rev. A* **89**, 023619 (2014).
- [33] S. Greschner, M. Piraud, F. Heidrich-Meisner, I. P. McCulloch, U. Schollwöck, and T. Vekua, *Phys. Rev. Lett.* **115**, 190402 (2015).
- [34] K. Plekhanov, G. Roux, and K. Le Hur, *Phys. Rev. B* **95**, 045102 (2017).
- [35] M. Atala, M. Aidelsburger, M. Lohse, J. T. Barreiro, B. Paredes, and I. Bloch, *Nat. Phys.* **10**, 588 (2014).
- [36] T. Mishra, R. V. Pai, and S. Mukerjee, *Phys. Rev. A* **89**, 013615 (2014).
- [37] T. Mishra, S. Greschner, and L. Santos, *Phys. Rev. A* **91**, 043614 (2015).
- [38] E. Anisimovas, M. Račiūnas, C. Sträter, A. Eckardt, I. B. Spielman, and G. Juzeliūnas, *Phys. Rev. A* **94**, 063632 (2016).
- [39] S. D. Huber and E. Altman, *Phys. Rev. B* **82**, 184502 (2010).
- [40] T. Mishra, S. Greschner, and L. Santos, *Phys. Rev. B* **92**, 195149 (2015).
- [41] T. Tonegawa and I. Harada, *J. Phys. Soc. Jpn.* **56**, 2153 (1987).
- [42] S. Sarkar and D. Sen, *Phys. Rev. B* **65**, 172408 (2002).
- [43] L. Capriotti, F. Becca, S. Sorella, and A. Parola, *Phys. Rev. B* **67**, 172404 (2003).
- [44] M. Nakane, Y. Fukumoto, and A. Oguchi, *J. Phys. Soc. Jpn.* **75**, 114712 (2006).
- [45] D. Sen, B. S. Shastry, R. E. Walstedt, and R. Cava, *Phys. Rev. B* **53**, 6401 (1996).
- [46] S. Chen, H. Büttner, and J. Voit, *Phys. Rev. Lett.* **87**, 087205 (2001).
- [47] T. Nakamura and K. Kubo, *Phys. Rev. B* **53**, 6393 (1996).
- [48] S. de Léséleuc, V. Lienhard, P. Scholl, D. Barredo, S. Weber, N. Lang, H. P. Büchler, T. Lahaye, and A. Browaeys, *Science* **365**, 775 (2019).
- [49] T. Zhang and J. Gyu-Boong, *Sci. Rep.* **5**, 16044 (2015).
- [50] S. R. White, *Phys. Rev. Lett.* **69**, 2863 (1992).
- [51] U. Schollwöck, *Ann. Phys.* **326**, 96 (2011).
- [52] P. Calabrese and J. Cardy, *J. Stat. Mech.: Theory Exp.* (2004) P06002.
- [53] A. A. Nersisyan, A. O. Gogolin, and F. H. L. Eßler, *Phys. Rev. Lett.* **81**, 910 (1998).
- [54] A. Osterloh, L. Amico, G. Falci, and R. Fazio, *Nature (London)* **416**, 608 (2002).
- [55] G. Vidal, J. I. Latorre, E. Rico, and A. Kitaev, *Phys. Rev. Lett.* **90**, 227902 (2003).